Geophysical Research Letters

RESEARCH LETTER
10.1029/2022GL099247

Key Points:

- Combining viscous creep and rate-and-state friction in fault slip models limits the peak loading stress over the earthquake cycle
- Numerical and analytical models reproduce Gutenberg-Richter earthquake size-recurrence statistics, with a *b*-value linked to fault stress
- The interplay between loading stress and probabilistic fault locking provides an explanation for regional contrasts in *b*-value

Supporting Information:

Supporting Information may be found in the online version of this article.

Correspondence to:

A. Beall,
adambeall1@gmail.com

Citation:

Beall, A., van den Ende, M., Ampuero, J.-P., Capitanio, F. A., & Fagereng, Å. (2022). Linking earthquake magnitude-frequency statistics and stress in visco-frictional fault zone models. *Geophysical Research Letters*, *49*, e2022GL099247. https://doi.org/10.1029/2022GL099247

Received 26 APR 2022
Accepted 29 SEP 2022

Linking Earthquake Magnitude-Frequency Statistics and Stress in Visco-Frictional Fault Zone Models

Adam Beall[1,2], Martijn van den Ende[3], Jean-Paul Ampuero[3], Fabio A. Capitanio[2], and Åke Fagereng[1]

[1]School of Earth and Environmental Sciences, Cardiff University, Cardiff, UK, [2]School of Earth, Atmosphere and Environment, Monash University, Clayton, VIC, Australia, [3]Observatoire de la Côte d'Azur, Université Côte d'Azur, IRD, CNRS, Géoazur, Valbonne, France

Abstract The ability to estimate the likelihood of given earthquake magnitudes is critical for seismic hazard assessment. Earthquake magnitude-recurrence statistics are empirically linked to stress, yet which fault-zone processes explain this link remains debated. We use numerical models to reproduce the interplay between viscous creep and frictional sliding of a fault-zone, for which inter-seismic locking becomes linked to stress. The models reproduce the empirical stress-dependent earthquake magnitude distribution observed in nature. Stress is related to the likelihood a fault section is near frictional failure, influencing likely rupture lengths. An analytical model is derived of a fault consisting of identical patches, each with a probability of inter-seismic locking. It reproduces a similar magnitude-recurrence relationship, which may therefore be caused by probabilistic clustering of locked fault patches. Contrasts in earthquake statistics between regions could therefore be explained by stress variation, which has future potential to further constrain statistical models of regional seismicity.

Plain Language Summary The frequency of earthquakes with a given magnitude is empirically described by the Gutenberg-Richter law, where large earthquakes occur less frequently than small ones. Variations in magnitude distribution between regions have been correlated with the tectonic force acting on a fault. However, it is unclear which mechanism is responsible for this relationship, restricting its predictive capability. Here, we create computational models in which some portions of a fault can generate earthquakes and others can move slowly (not generating earthquakes). This slow movement acts to relax and limit the elastic forces that build up around the fault. This approach is used to reproduce realistic earthquake statistics, indicating that processes that limit the stress build-up between earthquakes may be responsible for the varying likelihoods of earthquake magnitudes observed in nature.

1. Introduction

One of the cornerstones of modern seismic hazard assessment is the ability to model statistical distributions of how often earthquakes of a given size occur in a region (Gerstenberger et al., 2020). This is typically modeled following the Gutenberg-Richter (G-R) law, where the number N of earthquakes of moment magnitude M_w or greater that occur in a specific region and time period is given by $\log(N) = a - bM_w$. a and b are empirical parameters, which vary between regions. For example, for thrust fault earthquakes, b is 0.75 at the Honshu subduction margin, Japan, and 1.07 at the Marianas margin (Bilek & Lay, 2018). Higher *b*-values indicate that the ratio of small to large earthquake rates is larger (large earthquakes are relatively less frequent).

A high *b*-value has been linked to low differential stress in laboratory experiments (Scholz, 1968). In nature, it has been correlated with extensional tectonic regimes (Schorlemmer et al., 2005), shallow earthquake hypocenters (Spada et al., 2013), regions hosting inter-seismic creep (Tormann et al., 2014) and periods following large earthquakes (Nuannin et al., 2005). These contexts are generally associated with relatively low differential stress. The G-R distribution of earthquake sizes is thought to reflect a power-law (fractal) distribution of material properties, fault lengths or stress in the Earth, based on physical models. (Ampuero et al., 2006; Dublanchet, 2020; Huang & Turcotte, 1988; Kanamori & Anderson, 1975; King, 1983; Mogi, 1967; Scholz, 1968). An increase in the stress loading a material with a power-law strength distribution results in a larger critically stressed fault area (Huang & Turcotte, 1988; Scholz, 1968), while still reproducing the G-R law, leading to a predicted decrease in *b*-value. However, this process is complicated by rupture dynamics over earthquake cycles. Shear-stress evolves

heterogeneously as fault segments slip, while also depending on loading conditions. Earthquakes may also propagate through regions that are unfavorable for earthquake nucleation, depending probabilistically on the magnitude and heterogeneity of fault stress and strength (Ampuero et al., 2006; Fang & Dunham, 2013; Galis et al., 2015; Ripperger et al., 2007). Earthquake cycle models can address these ambiguities by reproducing fault stress states that evolve self-consistently and can be used to study the controls on rupture for various fault structures, properties, and conditions. Such models have been used to reproduce the G-R law (Cattania, 2019; Dublanchet, 2020; Dublanchet et al., 2013; van den Ende et al., 2020), though an outstanding question is how they can reproduce the observed *b*-value dependence on stress.

Faults commonly include "creeping" regions where elastic strain does not accumulate (inter-seismic coupling is low) and seismic slip is less likely (Avouac, 2015), influencing the distribution of possible earthquake magnitudes. Creep may occur by stable frictional sliding or viscous mechanisms. We use the term creep to refer exclusively to viscous deformation, which is inferred from evidence of pressure solution creep (Gratier et al., 2013; Rutter, 1976) that operates within fault-zones at depths typically including, but not limited to, 5–20 km (Bos & Spiers, 2002). Fault segments with low inter-seismic coupling are inferred from *b*-values to deform at low deviatoric stress (Tormann et al., 2014), which could be explained by viscous stress relaxation. Building on these inferences, we hypothesize that the proportion of fault area that is creeping is related to both fault stress and *b*-value, explaining why these are linked in nature. We test this hypothesis by developing earthquake cycle models in which fault deformation occurs by a combination of frictional sliding and viscous creep. Visco-frictional fault-zones observed in nature are represented as a coupled fault and shear-zone, allowing us to explore how stress relaxation due to shear-zone deformation (or off-fault creep) influences earthquake size. Our modeled earthquake cycles involve a range of rupture dynamics that depend on this visco-frictional interplay. The resulting catalog of models reproduce the relationship between stress and *b*-value. We also interpret these results through comparison to an analytical model and demonstrate that it is the probability that a given fault segment is critically stressed that controls the modeled earthquake statistics.

2. Methodology

2.1. Numerical Model

We use the boundary element code QDYN (Luo et al., 2017) to model quasi-dynamic earthquake cycles. QDYN solves the time-and position-dependent slip and slip-rate of a planar fault embedded in two elastic half-spaces undergoing constant tectonic loading. Slip and slip-rate depend on the elastic stress-state, while also relieving accumulated stress, providing a non-linear relationship between stress and fault slip that may generate the spectrum of creep to seismic slip. The coupled fault and shear-zone system is modeled on a 2-D vertical plane as a 1-D thrust fault, neglecting along-strike variation, with a seismogenic zone of width $L_f = 30$ km. Along unbounded extensions of the fault beyond its seismogenic zone, a steady slip velocity of $v_p = 10^{-9}$ m s^{-1} is prescribed, representing plate motion of ~30 mm/yr. On the seismogenic zone, a visco-frictional rheology is assumed in which total fault slip rate is the sum of viscous (v_v) and frictional (v_f) slip rates, such that the weakest mechanism dominates: at any given point on the fault we have (for bulk shear stress τ and frictional and viscous stresses τ_f and τ_v, respectively, and state variable θ):

$$\tau = \tau_f(v_f, \theta) = \tau_v(v_v) \tag{1}$$

$$v = v_f + v_v \tag{2}$$

Frictional strength is assumed to follow the rate-and-state law (Equation S1 in Supporting Information S1), with frictional rate parameter $(a - b) = -0.011$, such that the fault would be velocity-weakening and potentially seismic in the absence of creep. The steady-state static and dynamic strengths S_f and S_d are defined as the frictional strengths prior to and during seismic sliding. They are $S_f = 60$ and $S_d = 37$ MPa, for the reference friction coefficient $\mu_0 = 0.6$, effective normal stress 100 MPa and calculated at steady slip rates of v_p and 1 m/s, respectively. We take S_f and S_d as constants for analysis, though they are an approximation as the models are not steady-state and ruptures may have partial stress drops. The earthquake nucleation length L_∞ (following Rubin & Ampuero, 2005, Text S1 in Supporting Information S1), the size a slip zone must reach to become unstable, is 316 m for the chosen frictional parameters. L_b is the length-scale near a rupture front over which frictional weakening occurs and is approximately 150 m. A model resolution of 29.3 m is chosen to resolve both processes.

Viscous deformation is assumed to be Newtonian, following $\tau_v = v_v \eta / W$, for viscosity η and shear-zone width W. Fault-zones typically consist of mixtures of blocks of varying strengths and sizes that follow fractal distributions (Fagereng & Sibson, 2010; Kirkpatrick et al., 2021). Accordingly, the shear-zone consists of patches with random lengths from a truncated power-law distribution with exponent $D = 1$, ranging from 10 to 100 m. Each patch has a uniform η which is chosen by assuming that $\log(\eta)$ follows a uniform random distribution between $\eta_{\min} = 10^{18}$ and $\eta_{\max} = 10^{20}$ Pa s. This reflects heterogeneity within the seismogenic zone inferred in nature (Fagereng & Sibson, 2010; Gratier et al., 2013) and microphysical models (Bos & Spiers, 2002). W is uniform along the fault and constant for a given simulation. This setup could equivalently represent uniform η and down-dip W heterogeneity.

The model reproduces seismic and aseismic slip (Figure 1), with a range of rupture sizes, depending on visco-frictional interaction. For each simulation, an earthquake catalog is compiled with moment magnitudes M_w computed by assuming that earthquake areas are circular.

As a consequence of the adopted rheology, there exists a critical viscosity η_c, where if a fault patch has $\eta > \eta_c$ it will be primarily inter-seismically locked and capable of accumulating elastic energy and possibly of nucleating earthquakes. The steady-state strength of the viscous material S_v is the stress at which it accommodates plate motion: $S_v = v_p \eta / W$. Inter-seismic elastic strain accumulation plateaus at a peak stress below the frictional steady-state strength S_f (i.e., tectonic deformation is fully accommodated by creep) if $S_v / S_f < 1$. The threshold $S_v / S_f = 1$ corresponds to $\eta = \eta_c$, giving:

$$\eta_c = \frac{S_f W}{v_p} \tag{3}$$

ϕ is the probability that a given patch will be inter-seismically locked ($\eta > \eta_c$). A collection of adjacent locked patches is termed an "effective asperity" (Figure 1a). ϕ is also approximately equivalent to the proportion of the fault consisting of effective asperities, converging to an exact agreement as the number of patches is increased. For the viscosity distribution of the reference model-set, the probability ϕ is:

$$\phi \equiv P(\eta \geq \eta_c) = \frac{\ln(\eta_{\max}) - \ln(\eta_c)}{\ln(\eta_{\max}) - \ln(\eta_{\min})} \tag{4}$$

ϕ is controlled by varying W (Equation 3) and therefore η_c (Equation 4). Variation of ϕ could be equivalently achieved by varying the normal stress or friction coefficient along the fault and therefore S_f, however this would also modify the earthquake nucleation length and stress drop, so we only vary W for simplicity. We could equally have changed v_p, but that would also affect the earthquake recurrence intervals. Note that the definitions of ϕ and η_c assume steady-state simulations. Our simulations are not steady-state and small proportions of viscous deformation can occur during inter-seismic periods, even for $\eta > \eta_c$. Inter-seismically creeping patches can experience some co-or post-seismic frictional sliding due to the elevated stresses of a propagating earthquake.

We simulate regional scale variations in loading conditions by changing the key parameter ϕ, as average fault shear stress is shown to vary proportionally with ϕ up to a critical stress threshold (Figure 2a). ϕ is varied from 0.1 to 1 by varying W from 1,000 to 10 m. We run three models with different randomized realizations of the viscosity distribution for each ϕ, generating statistically significant earthquake catalogs for b-value analysis and testing the sensitivity to the randomized distribution.

As fault shear stress varies spatially and temporally, we calculate the representative fault shear stress τ_{av} by calculating the spatially averaged shear stress for each time-step and then taking the temporal maximum (Figure S2 in Supporting Information S1). τ_{av} is typically the average stress prior to the largest earthquake. Model dynamics depend on the stress relative to fault strength, not on the absolute stress. Stress is non-dimensionalized as the ratio $\overline{\tau}_{\text{av}}$ between the average available static stress drop prior to the largest event (following the τ_{av} definition) and the strength drop (which is also the maximum possible stress drop):

$$\overline{\tau}_{\text{av}} = \frac{\tau_{\text{av}} - S_d}{S_f - S_d} \tag{5}$$

Further modeling methodology details are included in Text S1 of Supporting Information S1.

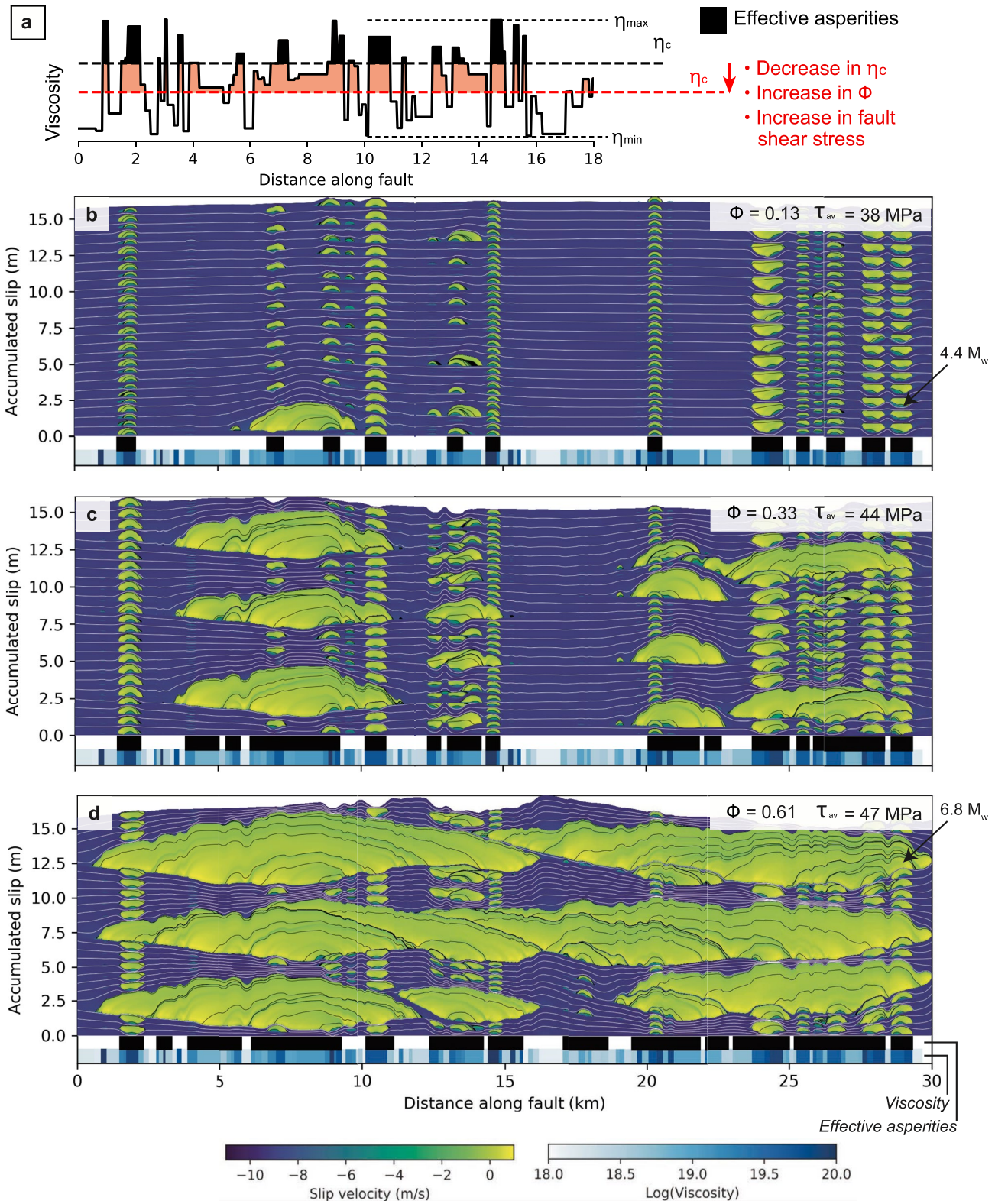

Figure 1. (a) Effective asperities occur where $\eta > \eta_c$ (shaded regions). (b–d) Modeled seismic (yellow) slip and creep (purple) accumulated over 500 years for reference models with various ϕ. White curves are separated by inter-seismic intervals of 20 years and black curves by seismic intervals of 2 s. Below each plot, the distributions of viscosity (identical between models) and effective asperities are shown.

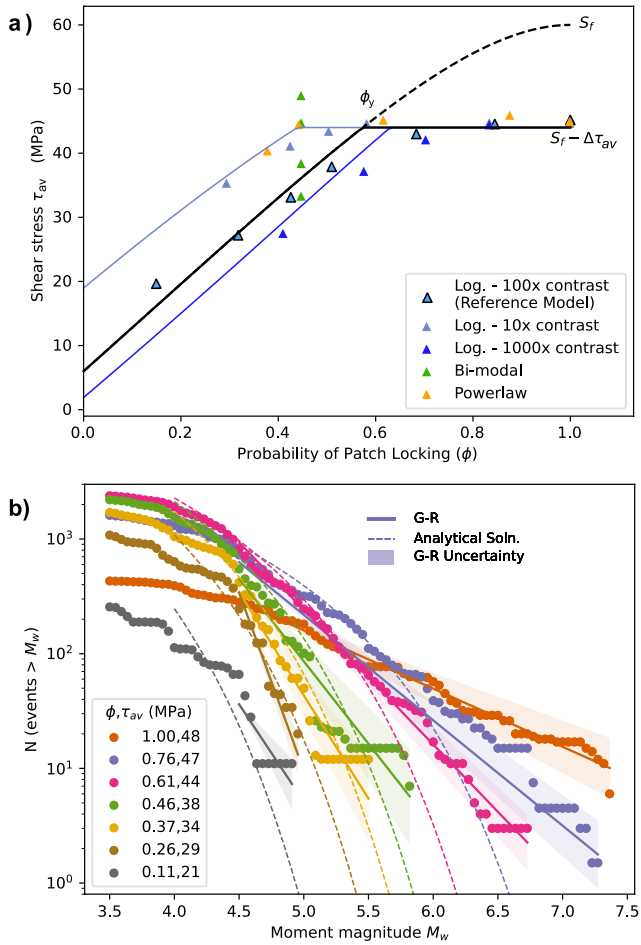

Figure 2. Variation of average shear stress (a) and magnitude statistics (b) between models with different patch locking probability ϕ. (a) Equation 7 is shown for the reference model-set (black line), with (solid) and without (dashed) capping at a stress $S_f - \Delta\tau_{av}$. Lower and higher viscosity contrasts are also shown by light and dark blue lines respectively. (b) The Gutenberg-Richter (G-R) fit (solid lines) and analytical solution (Equation 9) are shown (dashed lines).

2.2. Analytical Asperity Model

We construct a simplified analytical model for comparison. In this model the fault consists of many permanent patches of identical length w, each with a constant probability ϕ of steady-state inter-seismic locking and therefore of forming an effective asperity. The probability that a given effective asperity will consist of n patches is:

$$P(n) = (1-\phi)\phi^{n-1} \tag{6}$$

To predict the statistics of ruptures, we assume that each effective asperity repeatedly hosts events rupturing that individual asperity only. We assume that a single patch can nucleate an earthquake, which is justified by the fact that L_∞ is only 1.2x the length of the smallest patch. We take the patch length $w = 550$ m, which is the average patch length in the QDYN models. From this simple probabilistic model, we calculate estimates of the b-value (derivation fully described in Text S3 of Supporting Information S1).

3. Results

Models are run for 2,000 years, including a 500-year run-in period that is excluded from analysis. Earthquake stress drops are defined as the change in shear stress throughout an earthquake over the region it ruptured. Stress drops are relatively constant (standard deviation of 4 MPa) with an average $\Delta\tau_{av} = 17$ MPa (74% of the maximum possible strength drop $S_f - S_d$), within the range of seismological observations (Abercrombie, 1995). Events with $M_w > 5.5$ tend to have lower stress drops (~7 MPa), because large ruptures can pass through low stress regions, as discussed by Lambert et al. (2021).

The average stress τ_{av} increases linearly with increasing locking probability ϕ (Figure 2a), before plateauing at a peak value of approximately $S_f - \Delta\tau_{av}$. We define the value of ϕ where $\tau_{av} = S_f - \Delta\tau_{av}$ as ϕ_y. While $\tau_{av} < S_f$, fault segments locally reach S_f to nucleate earthquakes, which can propagate through regions with $\tau < S_f$. We also derive τ_{av} from the expected value of average viscosity (Text S3.1 in Supporting Information S1), giving Equation 7, which depends on the choice of viscosity contrast $\Delta\eta = \eta_{max}/\eta_{min}$ and agrees with the numerical results.

$$\tau_{av} \approx \begin{cases} \phi S_f + \dfrac{(1-\phi)S_f}{\Delta\eta^{0.5(1-\phi)}} & \phi < \phi_y \\ S_f - \Delta\tau_{av} & \phi \geq \phi_y \end{cases} \tag{7}$$

The relationship between ϕ and τ_{av} is therefore clear, where high fault-scale shear stress reflects an increased likelihood of patch locking.

At low ϕ and τ_{av}, earthquakes are generally limited to small isolated effective asperities (black stripes in Figure 1b). Earthquakes rarely propagate into adjacent creeping regions, and are restricted to low magnitudes ($M_w < 5.7$ and on average $M_w \sim 4$).

With increasing ϕ and consequently higher τ_{av}, effective asperities of increasing sizes can host larger earthquakes (Figures 1c and 1d), that also occasionally span multiple asperities. Small earthquakes also persist, both hosted on small effective asperities and occurring as partial ruptures of larger effective asperities. When $\phi = 0.61$, $\tau_{av} = 47$ MPa ($\overline{\tau}_{av} = 0.43$) and earthquakes with $M_w < 6.9$ occur, propagating through regions undergoing inter-seismic creep (interpreted as barriers) ≤1 km wide (Figure 1d). Large events occur less frequently than small events, and with greater displacement, as occurs in natural scaling relationships. The largest events in

the reference model-set occur when $\phi = 1$ ($W = 10$ m) and have $M_w < 7.4$, reaching the limit at which ruptures are restricted by fault length.

3.1. Magnitude Recurrence Distribution and *b*-Value

The recurrence times of seismic events are generally approximated by the G-R law (Figure 2b). This power-law is fit to the numerical data using a linear regression. Uncertainty is estimated by measuring the *b*-value for random subsets (1/3) of the data and taking the standard deviation. The minimum cut-off magnitude M_c for the G-R fit appears to be ~4.5, corresponding to a length-scale of 904 m, larger than the average patch length.

The *b*-value increases with decreasing ϕ and $\tau_{\max}$, reflecting the decreased likelihood of large events with decreasing stress. The exact *b*-value is ambiguous for $\phi \sim 0.1$, due to a small M_w range. Many *b*-values are within the range of *b*-values compiled by Nishikawa and Ide (2014) for subduction zones and all are within the wide range reported in the literature for all settings (El-Isa & Eaton, 2014). The maximum M_w increases approximately linearly with increasing ϕ, up to the occurrence of fault-spanning ruptures at $M_w \sim 7.5$ (see also Figure S3 in Supporting Information S1).

To understand the cause of this G-R law, we derive the magnitude recurrence distribution for the analytical asperity model (Text S3.1–3.4 in Supporting Information S1). The expected number of asperities having length L (assumed to be an integer multiple of w) or larger is:

$$E(W \geq L) = \frac{L_f(1-\phi)\phi^{\frac{L}{w}}}{w} \tag{8}$$

L_f is the total fault length and this prediction agrees with the numerical data (Figure S7 in Supporting Information S1). If each effective asperity ruptures repeatedly with stress drop $\Delta\tau$, the expected number of events with length larger than L is:

$$E(N \geq N_L) = \frac{(1-\phi)^2 \gamma \chi_a(\phi) L_f}{w^2} \sum_{n=L/w}^{\infty} \frac{\phi^n}{n} \tag{9}$$

for $\gamma = \mathrm{tv}_p G/(c_s \Delta\tau)$, geometric constant c_s, sampling duration t, shear modulus G and asperity seismic coupling χ_a. The infinite sum converges because $\phi < 1$, so large ruptures are increasingly improbable. Event length is converted to M_w, as $L \propto 10^{0.5 M_w}$ for constant $\Delta\tau$, giving the magnitude-recurrence relationship (dashed lines, Figure 2b). Equation 9 is not a power-law, instead tapering off at high M_w. It has a similar slope to the data and is a good approximation, but underestimates the number of large magnitude events when $\phi \geq 0.5$, likely because ruptures propagate between the effective asperities at high ϕ in the numerical models.

We find an equivalent *b*-value, by calculating the tangent of Equation 9, evaluated at a length-scale L (ideally slightly higher than the length-scale for M_c), giving:

$$b \equiv -\frac{\mathrm{d}\log_{10} E}{\mathrm{d}M_w} = \frac{L}{2w}\left(\frac{\sum_{k=0}^{\infty} \frac{\phi^k}{(k+L/w)^2}}{\sum_{k=0}^{\infty} \frac{\phi^k}{k+L/w}} - \ln\phi\right) \tag{10}$$

This expression is well approximated for $\phi < 0.95$ and $L/w \sim 1$ by:

$$b = \frac{1}{2} - 0.27\phi^2 - \frac{\mathrm{L}}{2\mathrm{w}}\ln(\phi) \tag{11}$$

This *b*-value only depends on ϕ and L/w. Equation 9 is tangent to the G-R law at $M_w = 5$ for the numerical models (Figure 2b), corresponding to $L = 1.6$ km, (compared to $w = 550$ m), giving $L/w = 3$. In this case, the *b*-value range of 2.5–0.3 in nature (El-Isa & Eaton, 2014) corresponds to $\phi = 0.26$ to 0.97.

Equation 11 reproduces the decrease of *b*-value with increasing ϕ, and agrees well with the numerical models (Figure 3a). The exact and approximate solutions are mostly indistinguishable. The *b*-value estimate is converted

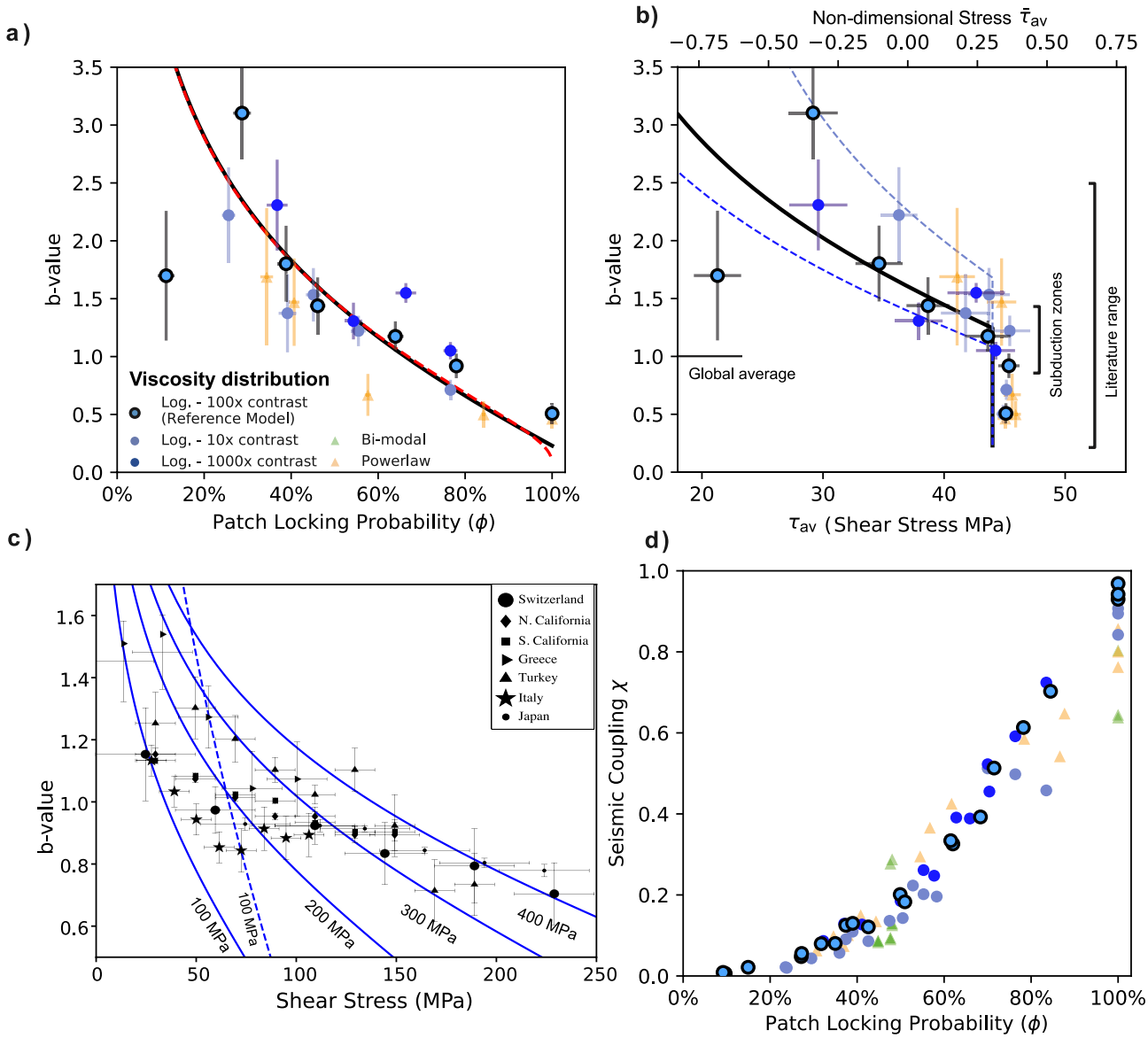

Figure 3. (a and b) b-value of the numerical models as a function of ϕ (a) and τ_{av} (b). Marker styles depict the reference model-set (outlined) and alternative viscosity distributions (see legend). The uncertainty in b-value fit and variation in τ_{av} within each set of random models are shown by vertical and horizontal bars. The bi-modal distribution model-set does not follow the Gutenberg-Richter distribution and is omitted. (a) The exact (red dashed line) and approximate (solid line) analytical predictions, Equations 10 and 11 are shown. (b) Equation 11 is shown as a function of stress (solid line), with light and dark blue dashed lines for smaller and larger viscosity contrasts. (c) Natural b-value estimates (modified from Scholz, 2015) are compared to Equation 11 (black line), assuming $L/w = 1$ and $\tau = m\phi$, where various values of m are labeled in MPa. A case $L/w = 3$ is also shown (dashed line). (d) Seismic coupling for all models (marker styles following a).

to a function of τ_{av} using Equation 7. The stress cut-off at $S_f - \Delta\tau_{av}$ explains the sharp decrease of b-value at $\tau_{av} = 43$ MPa ($\bar{\tau}_0 = 0.26$).

3.2. Viscosity Distribution Sensitivity

We tested the sensitivity of our results to the imposed viscosity probability distribution, using additional model-sets (symbols in Figure 3a, b, and 3d) with smaller or larger viscosity contrasts, or following power-law or bi-modal (either high or low viscosity) distributions (Text S2, Figure S4 in Supporting Information S1). The characteristics of these various models collapse onto similar curves when framed in terms of ϕ, as predicted by the analytical model. All model-sets approximately reproduce the G-R law, except the bi-modal distribution,

which is also bi-modal in M_w. Variation of statistics between model-sets arises when instead plotted in terms of shear stress, as also predicted by Equation 7.

4. Discussion

Our models analyze the underlying mechanism responsible for the variation of b-value with stress, observed experimentally and in nature. A fault with significant strength variation must be loaded to a relatively high stress for an earthquake to grow to a large magnitude, which has been interpreted to imply that relatively permanent fault properties, such as roughness, control both rupture characteristics and fault stress (Fang & Dunham, 2013). Loading stress depends on tectonic setting and can therefore contrast between faults. Dublanchet (2020) explored the influence of stress, varied by changing effective normal stress, on b-value in a rate-and-state earthquake cycle model, but found that this simultaneously affects the nucleation length and leads instead to an increase in b-value with increasing shear stress. We have modeled earthquake cycles on a fault-zone that can be loaded at arbitrary regional shear stresses, by incorporating viscous creep that limits the peak loading stress. Using this method, we can successfully reproduce the relationship between b-value and shear stress, without invoking variations in frictional properties.

The distribution of asperities and creeping regions on subduction megathrusts has been associated with geometrical and rheological heterogeneity at length scales of 100 m to 1 km (Kirkpatrick et al., 2020), which correspond to our modeled patches. Large earthquakes span distances of 10–100 km and variation in seismogenic behavior has been linked to geometric heterogeneity at such large wavelengths (van Rijsingen et al., 2018). Alternatively, large earthquakes may be hosted on many small asperities which rupture collectively at high stress (Tormann et al., 2014), corresponding to our modeled effective asperities. In this case, the distribution of earthquake sizes and nucleation sites depends on a combination of inherited properties at small scales and tectonic stress at larger scales. There is subsequently uncertainty in using asperity geometry to constrain the maximum M_w, as they may change effective size or link together with changing stress. The approximate reproduction of the G-R law with our analytical model with uniform patch lengths also indicates that the G-R law does not necessarily reflect power-law distributions of fault properties, but could be a statistical effect dependent on stress.

We propose that regional shear stress is linked locally to the probability ϕ that a fault segment is locked, which controls variations in earthquake statistics. Similar probabilistic dependence on stress has been proposed to explain b-value variation (Huang & Turcotte, 1988; Scholz, 1968), which we expand on by demonstrating its validity for an earthquake cycle model and with the derivation of a statistical model. In our numerical models ϕ is related to viscous creep, but the ability of our simplified viscosity-independent analytic model to reproduce similar statistics demonstrates that the link between earthquake statistics, ϕ and stress may be more general, explaining its occurrence in experimental data (Scholz, 1968) and nature (discussed next).

In Figure 3c we compare the derived b-value relationship to the natural data of Scholz (2015), who combined estimated tectonic stresses with b-value data from Spada et al. (2013). We apply a factor of 0.5 to their differential stress to convert it to invariant shear stress. The ∼100 MPa stresses shown are higher than the ∼10 MPa stress scale used in our models, maybe reflecting intra-plate stress compared to the lower stress on plate interfaces (Duarte et al., 2015). Our models only depend on the stress relative to frictional strength and can be rescaled. We assume that $\tau = m\phi$ (where m is an arbitrary constant), motivated by the linear relationship in our models (Figure 2a), though neglect the stress cut-off because there is no sharp b-value decrease at high stress in the data. We also assume $L = w$. Despite the simplifications of our asperity model, the natural decrease in b-value with increasing stress approximately follows the predicted logarithmic trend. An alternative case with $L > W$ overestimates the b-value variability with stress. Most of the data points are in the range $0.8 < b < 1.2$, for which the asperity model predicts that the probability of fault segments being inter-seismically locked or close to failure ranges from 25% to 55%, depending on stress. This is in contrast to the view that the crust is uniformly critically stressed (Townend & Zoback, 2000). Spatial variability in criticality, potentially corresponding to ϕ, was mapped by Langenbruch et al. (2018), who found that induced seismicity was more easily triggered in particular regions in the intra-plate USA.

ϕ may be inferred from estimates of seismic coupling χ (Figure 3d). We calculate χ as the ratio of the total accumulated seismic slip to the total loading displacement in the numerical models, which is equivalent to both seismic and inter-seismic coupling. χ is relatively insensitive to the choice of viscosity distribution and increases

monotonically with ϕ, though following a slightly non-linear relationship (detailed in Text S3.3 in Supporting Information S1).

Our models relate b-value and stress, providing future opportunities to integrate tectonic stress data into probabilistic seismic models. While the maximum M_w depends on stress in our models, it is underestimated by the asperity model, likely depending on more complex rupture dynamics. Intra-plate stress has plausible variation sufficient to cover a wider range of seismogenic behavior (Figure 3c). In subduction megathrusts, under-stressing may occur through the occurrence of pressure solution creep, which is ubiquitous in exhumed megathrusts (e.g., Fagereng & Sibson, 2010; Kirkpatrick et al., 2021). Geodynamic estimates indicate a ∼20% variation in plate interface shear stress between subduction regimes (Beall et al., 2021; Dielforder et al., 2020), which is sufficient to drive significant contrasts in seismicity in our numerical models. The inferred change in ϕ may then provide a mechanism to explain proposed variations of b-value with subduction stresses (Nishikawa & Ide, 2014; Scholz & Campos, 2012). As inter-seismic coupling is often well constrained in subduction zones from geodetic data, the link between ϕ and χ could also be used to constrain ϕ and test our model predictions as more geophysical observations become available.

5. Conclusions

We use numerical models to demonstrate that a visco-frictional fault with a heterogeneous distribution of viscously creeping and frictionally locked patches can host earthquakes that follow the G-R law. The modeling shows that the decreasing relative contribution of creep at higher driving stresses can explain the empirical link between b-value and stress. Analytical models indicate that this relationship can be interpreted more generally in terms of the probability that fault areas of various sizes are critically stressed. These first model applications highlight the potential to apply earthquake cycle models that incorporate stress-dependent inter-seismic locking in understanding regional contrasts in seismogenic behavior and earthquake statistics.

Data Availability Statement

The models described are available in an online repository at https://doi.org/10.5281/zenodo.6153898.

Acknowledgments
Analysis and plotting used the NumPy (Harris et al., 2020) and Matplotlib (Hunter, 2007) Python libraries. The acknowledge the following funding: European Union's Horizon 2020 research and innovation program, starting Grant 715836 MICA (AB, ÅF), support from Monash University (AB, FAC), French government supported UCAJEDI Investments in the Future project managed by the National Research Agency (ANR) Grant ANR-15-IDEX-01 (MPAvdE) and 3IA Côte d'Azur Investments in the Future project Grant ANR-19-P3IA-0002 (MPAvdE). We thank Baoning Wu for their constructive review.

References

Abercrombie, R. E. (1995). Earthquake source scaling relationships from −1 to 5 ML using seismograms recorded at 2.5-km depth. *Journal of Geophysical Research*, *100*(B12), 24015–24036. https://doi.org/10.1029/95JB02397

Ampuero, J. P., Ripperger, J., & Mai, P. M. (2006). Properties of dynamic earthquake ruptures with heterogeneous stress drop. In *Geophysical Monograph Series*.

Avouac, J.-P. (2015). From geodetic imaging of seismic and aseismic fault slip to dynamic modeling of the seismic cycle. *Annual Review of Earth and Planetary Sciences*, *43*(1), 233–271. https://doi.org/10.1146/annurev-earth-060614-105302

Beall, A., Fagereng, Å., Huw Davies, J., Garel, F., & Rhodri Davies, D. (2021). Influence of subduction zone dynamics on interface shear stress and potential relationship with seismogenic behavior. *Geochemistry, Geophysics, Geosystems*, *22*(2), e2020GC009267. https://doi.org/10.1029/2020gc009267

Bilek, S. L., & Lay, T. (2018). Subduction zone megathrust earthquakes. *Geosphere*, *14*(4), 1468–1500. https://doi.org/10.1130/ges01608.1

Bos, B., & Spiers, C. J. (2002). Frictional-viscous flow of phyllosilicate-bearing fault rock: Microphysical model and implications for crustal strength profiles. *Journal of Geophysical Research*, *107*, ECV1–13. https://doi.org/10.1029/2001JB000301

Cattania, C. (2019). Complex earthquake sequences on simple faults. *Geophysical Research Letters*, *46*(17–18), 10384–10393. https://doi.org/10.1029/2019gl083628

Dielforder, A., Hetzel, R., & Oncken, O. (2020). Megathrust shear force controls mountain height at convergent plate margins. *Nature*, *582*(7811), 225–229. https://doi.org/10.1038/s41586-020-2340-7

Duarte, J. C., Schellart, W. P., & Cruden, A. R. (2015). How weak is the subduction zone interface? *Geophysical Research Letters*, *42*(8), 2664–2673. https://doi.org/10.1002/2014gl062876

Dublanchet, P. (2020). Stress-dependent b value variations in a heterogeneous rate-and-state fault model. *Geophysical Research Letters*, *47*(13), e2020GL087434. https://doi.org/10.1029/2020gl087434

Dublanchet, P., Bernard, P., & Favreau, P. (2013). Interactions and triggering in a 3-D rate-and-state asperity model. *Journal of Geophysical Research: Solid Earth*, *118*, 2225–2245. https://doi.org/10.1002/jgrb.50187

El-Isa, Z. H., & Eaton, D. W. (2014). Spatiotemporal variations in the b-value of earthquake magnitude-frequency distributions: Classification and causes. *Tectonophysics*, *615–616*, 1–11. https://doi.org/10.1016/j.tecto.2013.12.001

Fagereng, Å., & Sibson, R. H. (2010). Mélange rheology and seismic style. *Geology*, *38*(8), 751–754. https://doi.org/10.1130/g30868.1

Fang, Z., & Dunham, E. M. (2013). Additional shear resistance from fault roughness and stress levels on geometrically complex faults. *Journal of Geophysical Research: Solid Earth*, *118*, 3642–3654. https://doi.org/10.1002/jgrb.50262

Galis, M., Pelties, C., Kristek, J., Moczo, P., Ampuero, J. P., & Mai, P. M. (2015). On the initiation of sustained slip-weakening ruptures by localized stresses. *Geophysical Journal International*, *200*(2), 888–907. https://doi.org/10.1093/gji/ggu436

Gerstenberger, M. C., Marzocchi, W., Allen, T., Pagani, M., Adams, J., Danciu, L., et al. (2020). Probabilistic seismic hazard analysis at regional and National scales: State of the art and future challenges. *Reviews of Geophysics*, *58*(2), 1–49. https://doi.org/10.1029/2019rg000653

Gratier, J. P., Thouvenot, F., Jenatton, L., Tourette, A., Doan, M. L., & Renard, F. (2013). Geological control of the partitioning between seismic and aseismic sliding behaviours in active faults: Evidence from the Western Alps, France. *Tectonophysics*, *600*, 226–242. https://doi.org/10.1016/j.tecto.2013.02.013

Harris, C. R., Millman, K. J., van der Walt, S. J., Gommers, R., Virtanen, P., Cournapeau, D., et al. (2020). Array programming with NumPy. *Nature*, *585*(7825), 357–362. https://doi.org/10.1038/s41586-020-2649-2

Huang, J., & Turcotte, D. L. (1988). Fractal distributions of stress and strength and variations of b-value. *Earth and Planetary Science Letters*, *91*(1), 223–230. https://doi.org/10.1016/0012-821x(88)90164-1

Hunter, J. D. (2007). Matplotlib: A 2D graphics environment. *Computing in Science & Engineering*, *9*(3), 90–95. https://doi.org/10.1109/mcse.2007.55

Kanamori, H., & Anderson, D. L. (1975). Theoretical basis of some empirical relations in seismology. *Bulletin of the Seismological Society of America*, *65*(5), 1073–1095.

King, G. (1983). The accommodation of large strains in the upper lithosphere of the Earth and other solids by self-similar fault systems: The geometrical origin of b-value. *Pure and Applied Geophysics*, *121*(5), 761–815. https://doi.org/10.1007/BF02590182

Kirkpatrick, J. D., Edwards, J. H., Verdecchia, A., Kluesner, J. W., Harrington, R. M., & Silver, E. A. (2020). Subduction megathrust heterogeneity characterized from 3D seismic data. *Nature Geoscience*, *13*(5), 369–374. https://doi.org/10.1038/s41561-020-0562-9

Kirkpatrick, J. D., Fagereng, Å., & Shelly, D. R. (2021). Geological constraints on the mechanisms of slow earthquakes. *Nature Reviews Earth & Environment*, *2*(4), 285–301. https://doi.org/10.1038/s43017-021-00148-w

Lambert, V., Lapusta, N., & Faulkner, D. (2021). Scale dependence of earthquake rupture prestress in models with enhanced weakening: Implications for Event Statistics and Inferences of Fault Stress. *Journal of Geophysical Research: Solid Earth*, *126*, e2021JB021886. https://doi.org/10.1029/2021jb021886

Langenbruch, C., Weingarten, M., & Zoback, M. D. (2018). Physics-based forecasting of man-made earthquake hazards in Oklahoma and Kansas. *Nature Communications*, *9*(1), 3946. https://doi.org/10.1038/s41467-018-06167-4

Luo, Y., Ampuero, J. P., Galvez, P., Ende, M. V. D., & Idini, B. (2017). QDYN: A Quasi-DYNamic earthquake simulator (v1.1).

Mogi, K. (1967). Earthquakes and fractures. *Tectonophysics*, *5*(1), 35–55. https://doi.org/10.1016/0040-1951(67)90043-1

Nishikawa, T., & Ide, S. (2014). Earthquake size distribution in subduction zones linked to slab buoyancy. *Nature Geoscience*, *7*(12), 904–908. https://doi.org/10.1038/ngeo2279

Nuannin, P., Kulhanek, O., & Persson, L. (2005). Spatial and temporal b value anomalies preceding the devastating off coast of NW Sumatra earthquake of December 26, 2004. *Geophysical Research Letters*, *32*(11), L11307. https://doi.org/10.1029/2005GL022679

Ripperger, J., Ampuero, J. P., Mai, P. M., & Giardini, D. (2007). Earthquake source characteristics from dynamic rupture with constrained stochastic fault stress. *Journal of Geophysical Research*, *112*, B04311. https://doi.org/10.1029/2006jb004515

Rubin, A. M., & Ampuero, J. P. (2005). Earthquake nucleation on (aging) rate and state faults. *Journal of Geophysical Research*, *110*, B11312. https://doi.org/10.1029/2005jb003686

Rutter, E. (1976). A discussion on natural strain and geological structure-the kinetics of rock deformation by pressure solution. *Philosophical Transactions of the Royal Society of London - Series A: Mathematical and Physical Sciences*, *283*(1312), 203–219.

Scholz, C. H. (1968). The frequency-magnitude relation of microfracturing in rock and its relation to earthquakes. *Bulletin of the Seismological Society of America*, *58*(1), 399–415. https://doi.org/10.1785/bssa0580010399

Scholz, C. H. (2015). On the stress dependence of the earthquake b value. *Geophysical Research Letters*, *42*(5), 1399–1402. https://doi.org/10.1002/2014gl062863

Scholz, C. H., & Campos, J. (2012). The seismic coupling of subduction zones revisited. *Journal of Geophysical Research*, *117*, B05310. https://doi.org/10.1029/2011jb009003

Schorlemmer, D., Wiemer, S., & Wyss, M. (2005). Variations in earthquake-size distribution across different stress regimes. *Nature*, *437*(7058), 539–542. https://doi.org/10.1038/nature04094

Spada, M., Tormann, T., Wiemer, S., & Enescu, B. (2013). Generic dependence of the frequency-size distribution of earthquakes on depth and its relation to the strength profile of the crust. *Geophysical Research Letters*. https://doi.org/10.1002/grl.50093

Tormann, T., Wiemer, S., & Mignan, A. (2014). Systematic survey of high-resolution b value imaging along Californian faults: Inference on asperities. *Journal of Geophysical Research: Solid Earth*, *119*, 2029–2054. https://doi.org/10.1002/2013jb010867

Townend, J., & Zoback, M. D. (2000). How faulting keeps the crust strong. *Geology*, *28*(5), 399–402. https://doi.org/10.1130/0091-7613(2000)28<399:HFKTCS>2.0.CO;2

van Rijsingen, E., Lallemand, S., Peyret, M., Arcay, D., Heuret, A., Funiciello, F., & Corbi, F. (2018). How subduction interface roughness influences the occurrence of large interplate earthquakes. *Geochemistry, Geophysics, Geosystems*, *12*(1), 2342–2370. https://doi.org/10.1029/2010gc003230

van den Ende, M. P. A., Chen, J., Niemeijer, A. R., & Ampuero, J. P. (2020). Rheological transitions facilitate fault-spanning ruptures on seismically active and creeping faults. *Journal of Geophysical Research: Solid Earth*, *125*, 1–27. https://doi.org/10.1029/2019jb019328

References From the Supporting Information

Rice, J. R. (1993). Spatio-temporal complexity of slip on a fault. *Journal of Geophysical Research*, *98*(B6), 9885. https://doi.org/10.1029/93jb00191

Rice, J. R., & Ben-Zion, Y. (1996). Slip complexity in earthquake fault models. *Proceedings of the National Academy of Sciences of the United States of America*, *93*(9), 3811–3818. https://doi.org/10.1073/pnas.93.9.3811